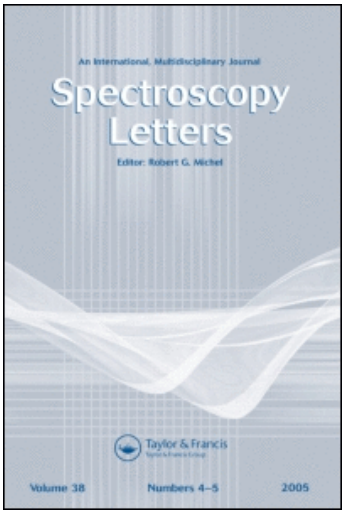

Spectroscopy Letters
Publication details, including instructions for authors and subscription information:
http://www.informaworld.com/smpp/title~content=t713597299

LASER INDUCED BUBBLE FORMATION AS A DAMAGE MECHANISM IN THE RETINAS OF MONKEY AND RABBIT

K. Sentrayan[a]; C. Haridass[b]; C. O. Trouth[a]
[a] Department of Neurology, Howard University Hospital, Washington, DC, U.S.A. [b] Department of Physical Sciences, Belfry High School, Belfry, Kentucky, U.S.A.

Online publication date: 31 July 2001

To cite this Article Sentrayan, K. , Haridass, C. and Trouth, C. O.(2001) 'LASER INDUCED BUBBLE FORMATION AS A DAMAGE MECHANISM IN THE RETINAS OF MONKEY AND RABBIT', Spectroscopy Letters, 34: 4, 469 — 494
To link to this Article: DOI: 10.1081/SL-100105094
URL: http://dx.doi.org/10.1081/SL-100105094

SPECTROSCOPY LETTERS, 34(4), 469–494 (2001)

LASER INDUCED BUBBLE FORMATION AS A DAMAGE MECHANISM IN THE RETINAS OF MONKEY AND RABBIT

K. Sentrayan,[1,3,*] C. Haridass,[2] and C. O. Trouth[1,3]

[1]Department of Neurology, Howard University Hospital, 2041 Georgia Ave. N.W. Washington, DC 20060, USA
[2]Department of Physical Sciences, Belfry High School, Belfry, Kentucky 41514, USA
[3]Department of Physiology and Biophysics, Howard University, College of Medicine, Washington, DC 20059, USA

ABSTRACT

We have used a model to investigate the damage mechanism in the retinas of monkeys and rabbits due to bubble formation induced by lasers at 0.514 μm, 0.633 μm, 0.694 μm and 1.06 μm with pulse duration in the sub-micro-second regime. In this model, the main absorbers are the melanosomes in the retinal pigment epithelium (RPE) which are surrounded by a non-absorbing cellular medium with thermal characteristics of water. The growth of the bubble was calculated from the experimentally derived values reported in the literature for the

*Corresponding author.

absorption coefficient of melanosomes using the ideal gas law under adiabatic conditions. Our calculated ED_{50} values are 2.235 J cm^{-2} (0.514 μm), 4.484 J cm^{-2} (0.633 μm), 7.420 J cm^{-2} (0.694 μm), 32.870 J cm^{-2} (1.060 μm) for monkey; 3.550 J cm^{-2} (0.514 μm), 6.770 J cm^{-2} (0.633 μm), 10.510 J cm^{-2} (0.694 μm) and 45.710 J cm^{-2} (1.06 μm) for rabbit considering that the shape of the RPE cell is hexagonal. The ED_{50} values reported in the present work are 18.2% and 74.9%, higher than those reported by Birngruber *et al.*, for monkey and rabbit, respectively at laser wavelength 1.060 μm. This increase narrows to 8% and 71% for monkey and rabbit, respectively when van der Waals equation of state is used to calculate the energy (q) required to raise 1 gm of "water-like" cellular medium surrounding the melanosome from body temperature (37^{E}C) at 1 atm. pressure to the critical point (374^{E}C) at 218 atm. pressure. Differences between our calculated ED_{50} values and that of the experimental values of other investigators may be attributed to wide variations in their measurements of the retinal image size. In addition, our estimation of retinal radiant exposure from the threshold energy and retinal image size is based on the assumption that the beam profile is gaussian (TEM_{00}). Our results suggest that the thermodynamic model using the van der Waals equation of state may predict more accurately the laser induced retinal damage due to bubble formation than the model using the ideal gas equation.

Key Words: Ocular injury; Melanosomes; Retinal pigmental epithelium; Q-switched lasers; ED_{50} measurements

INTRODUCTION

The widespread use of Q-switched high power, ultrashort laser pulses for various procedures in medicine and surgery has lead to a possible increase in the risk of ocular injury[1–11]. Ultraviolet (UV) lasers with wavelengths less than 200 nm (energy per photon greater than 6 eV) cause non-thermal ablation[12]. In this process, the laser photon energy is absorbed by tissue bio-molecules exciting the electronic states that lie above the dissociation energy of the molecular bands leading thereby to splitting of larger polymer chains into small fragments. Breaking of bonds causes an increase in pressure inside the laser irradiated tissue, and this causes

molecular fragments to escape from the tissue. Visible and infrared (IR) lasers mainly heat the tissue. The thermal damage in living cells induces deactivation of enzymes or denaturation of proteins thereby disturbing the genetic apparatus of the cell[13]. For pulse lengths longer than 10^{-5} s, an Arrhenius-type activation process is considered to be the dominant thermal damage mechanism[14]. The nano-second and pico-second laser pulses induce optical breakdown (plasma) in the tissue and this is called as photo-disruption in clinical ophthalmology. After a certain degree of ionization has been reached, the plasma undergoes sudden expansion accompanied by mechanical (acoustic) shock waves, which propagate with supersonic velocities[15–18]. The tissue damage due to the shock waves induced by laser pulses has been assessed using polymer films as tissue models[19–21], cells[22,23] and skin[24]. It has been reported that the threshold energy for optical breakdown is proportional to the square root of the pulse duration of the laser in ocular medium[25,26]. This indicates that optical breakdown can be very easily achieved at much lower energies with femto-second laser pulses compared to the nano-second and pico-second laser pulses. However, for pulse duration less than 10^{-6} s, damage can occur at the cellular level due to bubble formation[27,28]. It is interesting to note that the long pulse laser (250 μs) causes continued vaporization after the initiation of the bubble, producing a pear-shaped bubble[29,30], whereas the laser pulse less than 1 ns duration produces a spherical bubble[31]. It has been reported that more than 95% of all eye injuries (with vision loss) result from short pulse, Q-switched Nd:YAG lasers[32]. Hence it has become important to understand the damage mechanism in the time of 10^{-6} s or shorter of the Q-switched laser pulses.

Gerstman *et al.*[33] modeled the thermodynamic aspects of absorption of laser pulses by the melanosomes in the retinal pigment epithelium (RPE) surrounded by a water-like cellular medium, to understand the underlying physical damage mechanism due to bubble formation. The authors followed the work of Cleary[34] in which the initial pressure at the end of the laser pulse was taken to be the critical pressure of water ($P_c = 218$ atm). The growth of the bubble was calculated under adiabatic conditions using the ideal gas law. In the present work, we have used the ideal gas law and included the realistic experimental values of absorption coefficient (α) at 0.514 μm, 0.694 μm, 0.633 μm and 1.060 μm laser wavelengths for monkey and rabbit and the melanosome radius to predict the damage mechanism in the retinas of monkey and rabbit from the laser induced bubble formation. In an attempt to improve the model, we have used the Van der Waals equation of state to calculate the energy (q) required to raise 1 gm of "water-like" cellular medium surrounding the melanosome from body temperature (37 °C) at 1 atm. pressure to the critical point (374 °C) at 218 atm. pressure.

ED_{50} values are calculated from the radius of the damaging spheres due to bubble growth and compared with the experimentally observed values.

THEORETICAL DESCRIPTION

The Model

In this model the main absorbers are the melanosomes in the retinal pigment epithelium (RPE) surrounded by a non-absorbing cellular medium with the thermal characteristics of water. The retinal pigment epithelium cells investigated for the species human, monkey, rat, sheep, rabbit, cow, dog and chicken were observed to exhibit a high degree of regularity in terms of uniformity of the size, shape and pigmentation[35]. The RPE cells are hexagonal in shape. In most of the above-mentioned species the cells are mononuclear. The RPE contains two types of pigments namely, lipofuscin and melanin[36]. Lipofuscin is found to be almost absent in fetal and newborn RPEs and in the RPEs of aged eyes it is often found combined with melanin in the form of melanolipofuscin granules[37,38]. This has been confirmed by the observation of age related spectral modification in melanin due to a progressive accumulation of lipofuscin in the granule[39].

In this work, we investigate the laser induced damage mechanism in the retinas of monkey and rabbit. The diameter of the melanin in the granules of the pigment epithelium of the retina of the rabbit is 0.5 μm and in monkeys there exists two types of pigment granule, globular (0.5 μm in diameter) and elongated (dimension: 0.5×1.5 to 2.0 μm)[40]. A schematic representation of the vertical section of the retina of rabbit and monkey illustrating the approximate dimensions are shown in Fig. 1.A and Fig. 1.B, respectively[41,42].

Considering the diameter (d) of globular pigment granule into the rabbit and monkey RPE as 0.5 μm, the speed of heat conduction surrounding the water-like medium is given by[33]:

$$V_{\text{thermal}} \sim \frac{K_w}{\rho_w C_w d} \approx \frac{0.57\left(\frac{J}{ms\,^{\circ}C}\right)}{10^3\left(kgm^{-3}\right) \times 4.19 * 10^3\left(\frac{J}{kg\,^{\circ}C}\right) \times 0.5 * 10^{-6}(m)} \approx 0.2\left(\frac{m}{s}\right) \quad (1)$$

where K_w, Δ_w and C_w are thermal conductivity, density and heat capacity of water, respectively. Based on the dimension of the choroid of rabbit[41] and monkey[42], for sub-microsecond ($< 10^{-6}$ s) laser pulses, the heat wave will travel a distance < 0.2 μm from the melanosomes in the RPE of rabbit and

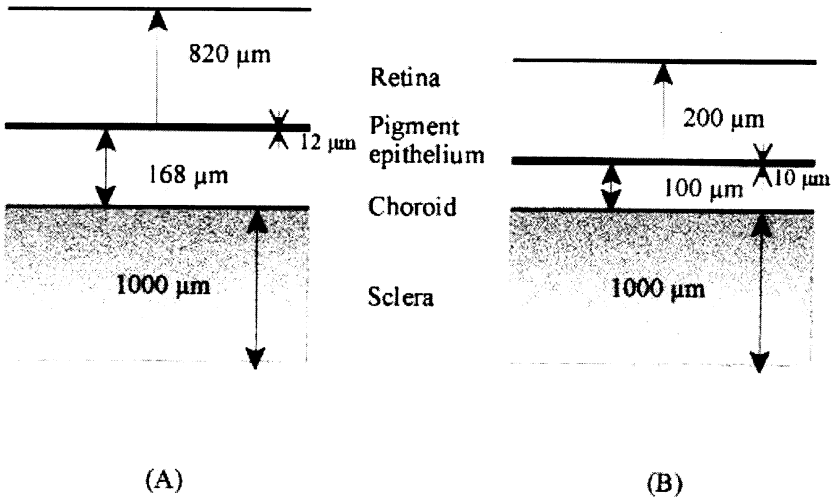

Figure 1. (*A*) A schematic representation of the vertical section through a rabbit retina illustrating the approximate dimension[41]. (*B*) A schematic representation of the vertical section through a rhesus monkey illustrating the approximate dimension[42].

$< 0.5\,\mu m$ from the melanosomes in the RPE of monkey. Hence it is responsible to assume that the heat wave will not reach the choroid and it is unlikely that the choroid will be damaged. Since there is no heat loss during laser absorption and subsequent bubble growth, an adiabatic approximation can be used to calculate an important parameter like radius to characterize the growth of the bubble. Following the treatment of Gerstman *et al.*,[33] the maximum radius of the bubble can be expressed in terms of the radius of the melanosome "a", absorption coefficient α and laser energy fluence H_0 as

$$r_{max} = a\left\{1 + \left[\frac{3}{4\pi a^3}\left(\frac{E - E_m}{q\rho_c}\right)\right]\left(\frac{P_1}{P_{min}}\right)^{\frac{1}{7}}\right\}^{\frac{1}{3}} \tag{2}$$

where E is the total energy absorbed by a spherical absorber of radius "a" and absorption coefficient α and is given by:

$$E = \pi a^2 H_0\left(1 - \frac{1}{2\alpha^2 a^2}\left[1 - e^{-2\alpha a}(1 + 2\alpha a)\right]\right). \tag{3}$$

Here, E_m is the energy required to raise a melanosome from 37 °C to 374 °C and is equal to

$$c_m \rho_m \left(\frac{4\pi}{3}\right) a^3 \Delta T \tag{4}$$

where c_m and Δ_m are the specific heat and density, respectively, of the melanin. The value of c_m and Δ_m are $2.51\,J(g\,^\circ C)^{-1}$ and $1.35\,g\,cm^{-3}$, respectively; q is the energy required to raise 1 gm of water from 37 °C at 1 atmosphere to 374 °C at 218 atmospheres. Gerstman *et al.*[33] used the ideal gas law to calculate q. In the present investigation we used Van der Waals equation of state to calculate q and the details are given in the Appendix; Δ_c is the density of water at the critical point, equal to $0.315\,g\,cm^{-3}$; P_1 is the pressure at the end of the laser pulse equal to the critical pressure of water (218 atmospheres); P_{min} is the minimum pressure at which the bubble stops expanding and is the ambient pressure that is equal to 1 atmosphere; (is the ratio between specific heat at constant pressure and specific heat at constant volume and is equal to 1.333.

RESULTS AND DISCUSSION

The energy absorbed by the melanosomes from the laser pulse is calculated using Eq. (3) and plotted as a function of retinal radiant exposure in Figs. 2 and 3 for monkey and rabbit, respectively. The figures indicate that as the retinal radiant exposure increases, the energy absorbed by the melanosome also increases for a given laser wavelength[8] and fixed radius ($a = 0.25\,\mu m$) of the melanosome. The energy absorbed by the melanosome is the highest at the wavelength of Ar^+ laser ($0.514\,\mu m$) and the lowest for the Nd:YAG laser ($1.060\,\mu m$). The energy absorption characteristics mentioned above are in general similar for both monkey and rabbit. The slope of the line of melanosome energy absorption versus retinal radial exposure was determined by fitting to a linear regression and is given in Figs. 2 and 3. In the present work, we have estimated the bracketed term in Eq. (3) which is represented as $C(\alpha,a)$ by Gerstman *et al.*[33]. Using the values for $\forall$ of melanin for both monkey and rabbit, the values of $C(\alpha,a)$ were calculated and compared with approximated second order term represented by $C_{\alpha,a} \cdot \left[\frac{4}{3}\alpha a - (\alpha a)^2\right]$. The comparison between $C(\alpha,a)$ is given in Table 1. We have also estimated the ratio of the slopes for both monkey and rabbit and the values are 0.9529 ($0.514\,\mu m$), 0.9051 ($0.694\,\mu m$), 0.8492 ($0.633\,\mu m$) and 0.8336 ($1.060\,\mu m$). It is clear from these values that as the wavelength increases the ratio of the slope for both monkey and rabbit decreases.

In the present work, to understand the dependency of the absorption coefficient on the total energy absorbed by melanosome, we have calculated the values of E/H_0 for four absorption coefficients using Eq. 3 for both

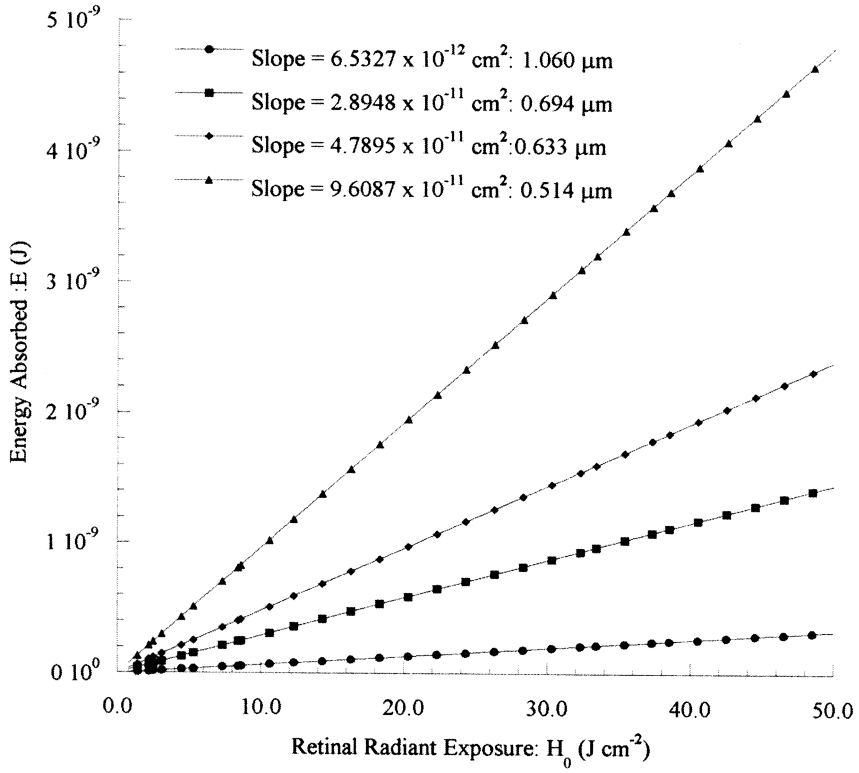

Figure 2. Laser energy absorbed by the melanosomes versus retinal radiant exposure for monkey at various laser wavelengths.

monkey and rabbit which are given in Table 2. From this table, it is evident that as the absorption coefficient increases the value E/H_0 also increases for both monkey and rabbit. This linear relationship between E/H_0 vs absorption coefficient is plotted in Fig. 4.

In the present work, the maximum radius of the bubble (r_{max}) at various retinal radiant exposures (H_0) was calculated inorder to understand the mechanism of cellular damage. The values are calculated using the expression given in Eq. (2). Our calculated values are more reliable than that of Gerstman *et al.*[33] since in our work, we have used the radius of melanosome to be 0.25 μm, and taken the experimental values of the absorption coefficient of melanosome at 0.514 μm , 0.694 μm, 0.633 μm and 1.060 μm laser wavelengths for both monkey and rabbit. These calculated values are plotted in Figs. 5 and 6 for both monkey and rabbit and selected values are

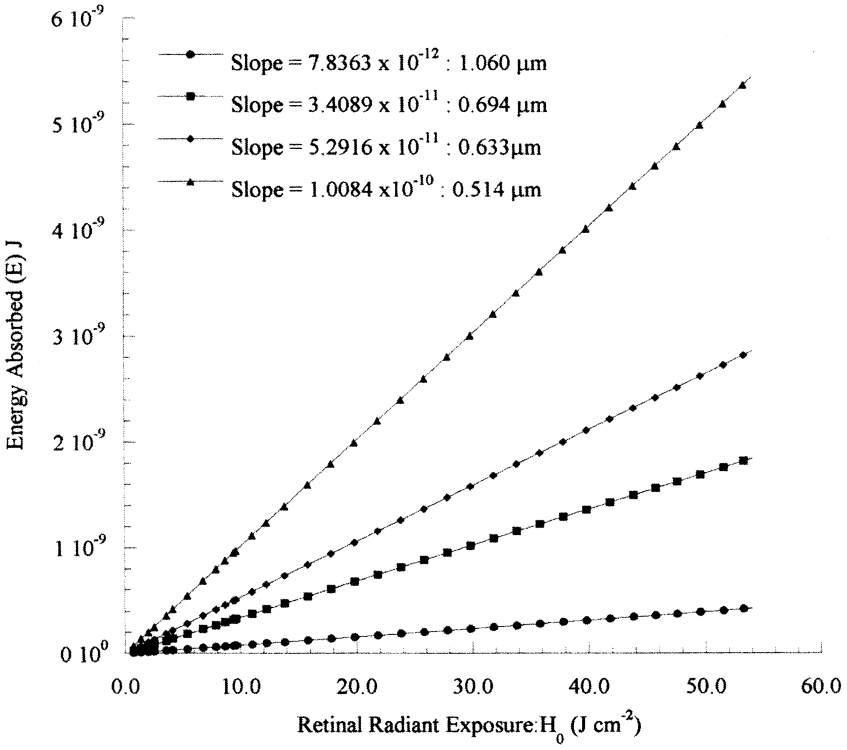

Figure 3. Laser energy absorbed by the melanosomes versus retinal radiant exposure for rabbit at various laser wavelengths.

Table 1. Accuracy of the Estimation of C(α,a) from Eq. (3) and Approximated Second Order Term for Both Monkey and Rabbit

Wavelength (nm)	α (cm^{-1})	a (μm)	C(α,a) in Eq. (3)	C(α,a)· $[4/3\alpha a-(\alpha\ a)^2]$	% Accuracy
			Monkey		
1.060	100	0.25	3.3271×10^{-3}	3.3271×10^{-3}	.000
0.694	446	0.25	1.4743×10^{-2}	1.4742×10^{-2}	.005
0.633	742	0.25	2.4393×10^{-2}	2.4389×10^{-2}	.014
0.514	1510	0.25	4.8937×10^{-2}	4.8908×10^{-2}	.058
			Rabbit		
1.060	120	0.25	3.9910×10^{-3}	3.9910×10^{-3}	.000
0.694	526	0.25	1.7362×10^{-2}	1.7360×10^{-2}	.007
0.633	821	0.25	2.6950×10^{-2}	2.6945×10^{-2}	.017
0.514	1587	0.25	5.1359×10^{-2}	5.1326×10^{-2}	.064

Table 2. Calculated E/H_0 Values for Four Different Absorption Coefficient for Both Monkey and Rabbit

Monkey		Rabbit	
α (cm^{-1})	E/H_0 (J)	α (cm^{-1})	E/H_0 (J)
100	6.533×10^{-12}	120	7.836×10^{-12}
446	2.895×10^{-11}	526	3.409×10^{-11}
742	4.789×10^{-11}	821	5.292×10^{-11}
1510	9.609×10^{-11}	1587	1.008×10^{-10}

given in Tables 3 and 4. It is evident from Eq. (2) that the bubble radius depends on the retinal radiant exposure, size of the melanosome, its absorption coefficient and thermal properties, namely, density and specific heat. From the figures presented, it is clear that for a given melanosome

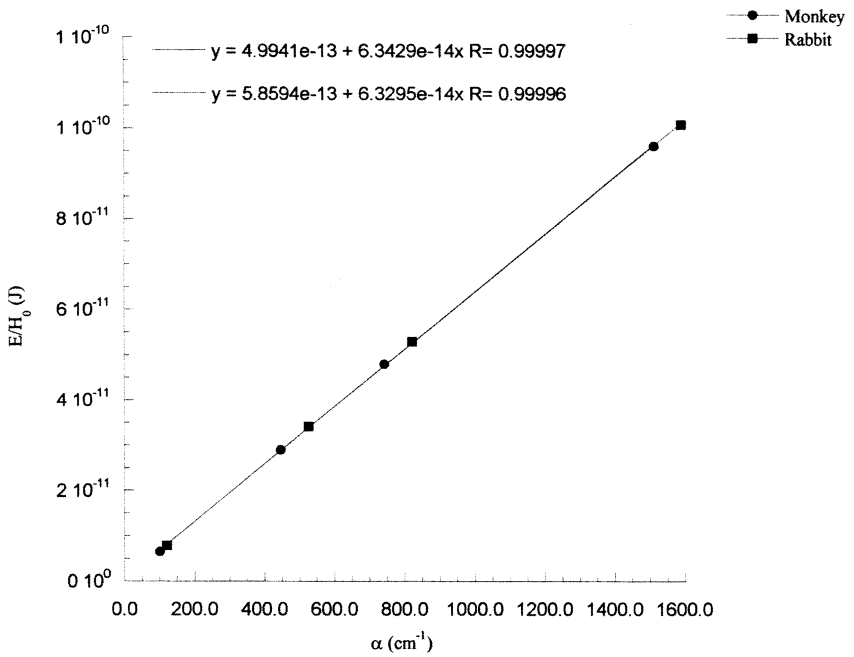

Figure 4. Variation in the ratio between energy absorbed by the melanosomes and the retinal radiant exposure with absorption coefficient of the melanosomes. R-represents the regression coefficient.

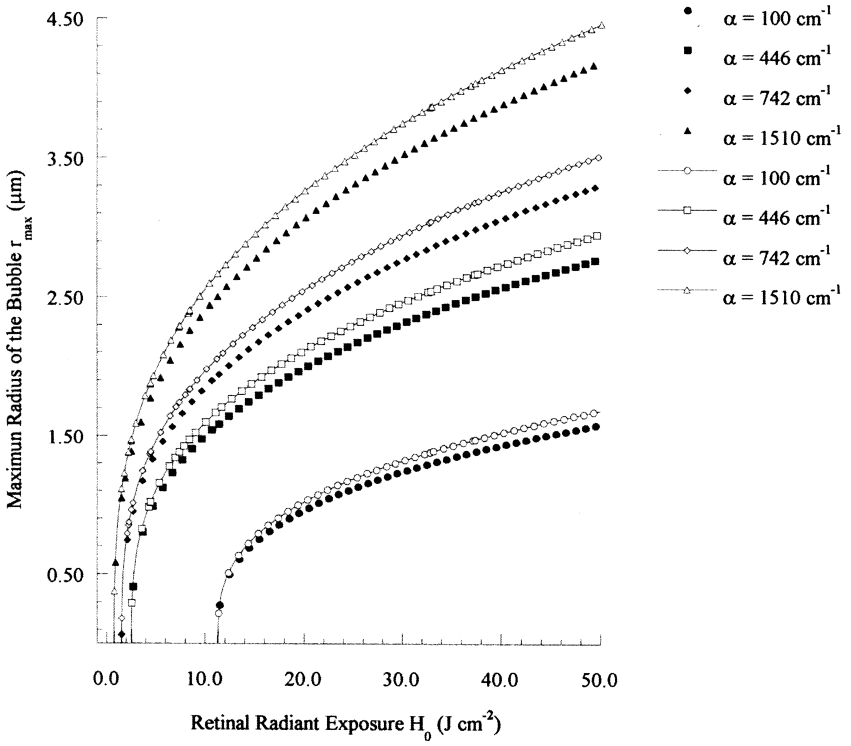

Figure 5. Maximum radius of the bubble versus retinal radiant exposure at different absorption coefficients of the melanosome for monkey. "Solid symbols" represents when q is calculated using ideal gas law. "Open symbols" represents when q is calculated using van der Waals equation of state.

radius and absorption coefficient, the bubble radius varies in a non-linear fashion with respect to retinal radiant exposure. The wavelength dependency of the bubble growth can be easily seen in Figs. 5 and 6, where the higher radius of the bubble corresponds to higher melanosome absorption coefficient. The damage criteria used in the present investigation can be explained as follows:

(1) The volume of the RPE cells of monkey and rabbit is calculated based on its dimensions given in Table 5[35]. (2) The number of melanosomes in an RPE cell is calculated as 51 by adding its contributions from three retinal zones namely macula, equator and periphery of human retinas given in Table 6[43]. Since melanin content decreases with age, the mean number of melanosomes per RPE cell is obtained from 50 human eyes, five from each

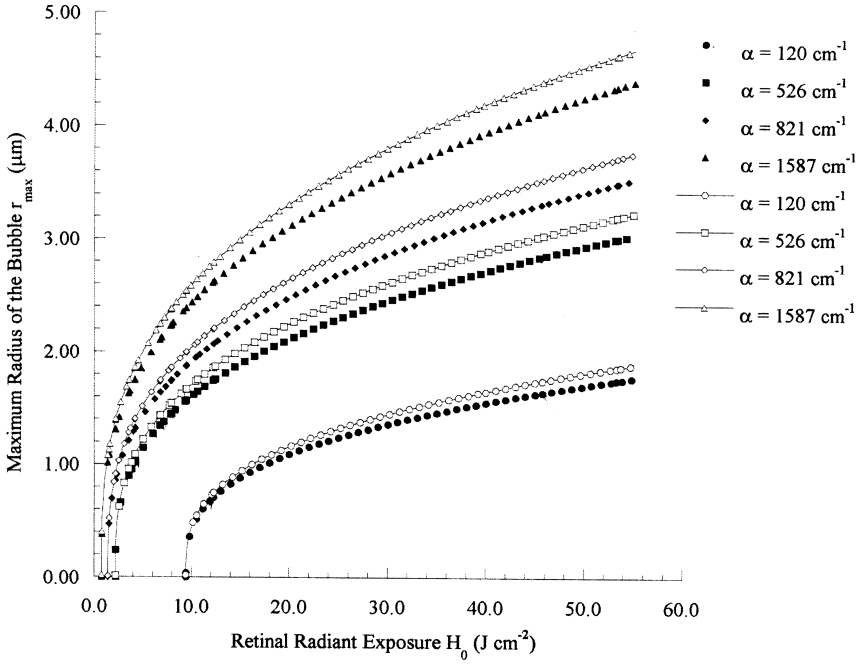

Figure 6. Maximum radius of the bubble versus retinal radiant exposure at different absorption coefficients of the melanosome for rabbit. "Solid symbols" represents when q is calculated using ideal gas law. "Open symbols" represents when q is calculated using van der Waals equation of state.

ten decades of life. Since the number of melanosomes in the RPE cells for monkey and rabbit are not available, in an effort to generate our first estimation we have used the values of human. The eye of a monkey displays the greatest similarity to the human eye in terms of geometrical form, optical power of refraction and anatomical structure of the retina. However, it has been found that there are considerable differences in fundus pigmentation, particularly in the choroid[44]. It is worth mentioning that in the present model for sub-microsecond pulses, heat wave will not reach the choroid therefore the choroid will not be affected. In chinchilla grey rabbits, the density and location of light absorbing pigments in the fundus are rather uniform and have close correspondence to that of the human eye[45]. (3) The volume of a melanosome of radius 0.25 μm is 0.0654 $(\mu m)^3$ (volume = $4/3Ba^3$). The total volume of 51 such melanosomes is 3.34 $(\mu m)^3$. (4) In order to compare the damage threshold value to ED_{50} measurements, the volume of the 51 such damaging spheres must occupy at least 50% of the

Table 3. Maximum Radius of the Bubble (r_{max}) at Various Retinal Radiant Exposure (H_0) for Monkey at Two Different q Values Calculated Using Ideal Gas Law and Van Der Waals Equation

r_{max} for $q = 2770$ J g^{-1}					r_{max} for $q = 2297$ J g^{-1}				
H_0 (J cm^{-2})	$\alpha = 100$ cm^{-1}	$\alpha = 446$ cm^{-1}	$\alpha = 742$ cm^{-1}	$\alpha = 1510$ cm^{-1}	H_0 (J cm^{-2})	$\alpha = 100$ cm^{-1}	$\alpha = 446$ cm^{-1}	$\alpha = 742$ cm^{-1}	$\alpha = 1510$ cm^{-1}
0.8				0.001	0.8				0.000
1.5			0.001	1.048	1.1				0.841
1.9			0.645	1.191	1.5			0.001	1.117
2.5		0.001	0.908	1.385	2.0			0.743	1.303
3.6		0.779	1.153	1.617	2.2			0.855	1.383
4.3		0.924	1.271	1.740	2.6		0.001	0.967	1.475
5.0		1.033	1.370	1.848	3.5		0.801	1.206	1.700
5.4		1.086	1.421	1.905	4.5		1.018	1.384	1.886
7.0		1.260	1.595	2.103	5.5		1.169	1.525	2.042
8.8		1.411	1.754	2.288	7.5		1.389	1.748	2.296
10.2		1.509	1.860	2.414	9.5		1.556	1.925	2.504
11.1		1.566	1.923	2.489	10.5		1.627	2.003	2.596
11.3	0.000	1.578	1.935	2.503	11.3	0.000	1.681	2.061	2.667
12.1	0.435	1.625	1.988	2.566	11.5	0.284	1.693	2.074	2.682
14.1	0.658	0.732	2.106	2.709	12.5	0.526	1.753	2.142	2.763
15.7	0.765	1.808	2.192	2.814	13.5	0.644	1.810	2.205	2.840
16.9	0.828	1.861	2.252	2.887	15.5	0.800	1.914	2.322	2.981
17.6	0.862	1.891	2.286	2.928	17.5	0.911	2.008	2.428	3.110
18.9	0.917	1.944	2.346	3.002	18.5	0.958	2.052	2.477	3.171
20.3	0.971	1.998	2.407	3.077	20.5	1.040	2.135	2.571	3.286
22.1	1.031	2.063	2.482	3.169	22.5	1.110	2.211	2.659	3.394
24.0	1.088	2.128	2.556	3.260	24.5	1.173	2.283	2.741	3.495

24.7	1.108	2.151	2.582	3.293	27.5	1.256	2.382	2.855	3.636
26.1	1.145	2.196	2.633	3.356	29.5	1.305	2.444	2.927	3.725
26.9	1.166	2.220	2.662	3.391	30.5	1.329	2.474	2.961	3.768
27.8	1.187	2.247	2.693	3.429	31.5	1.352	2.503	2.995	3.809
29.1	1.218	2.285	2.736	3.483	32.5	1.374	2.532	3.028	3.850
30.9	1.258	2.336	2.795	3.555	33.5	1.395	2.560	3.060	3.890
32.5	1.291	2.379	2.845	3.617	34.5	1.415	2.587	3.092	3.929
33.8	1.317	2.413	2.884	3.666	35.5	1.435	2.614	3.123	3.968
35.2	1.343	2.448	2.925	3.717	36.5	1.455	2.640	3.153	4.006
36.9	1.375	2.490	2.973	3.777	37.5	1.474	2.665	3.183	4.043
37.7	1.389	2.509	2.996	3.805	38.5	1.493	2.691	3.212	4.079
38.5	1.403	2.528	3.018	3.823	39.5	1.511	2.715	3.241	4.115
39.5	1.420	2.551	3.045	3.866	40.5	1.528	2.740	3.269	4.150
40.6	1.438	2.576	3.074	3.902	41.5	1.546	2.764	3.297	4.184
42.5	1.468	2.618	3.123	3.963	42.5	1.562	2.787	3.324	4.218
44.1	1.493	2.653	3.163	4.013	43.5	1.579	2.810	3.351	4.252
45.0	1.506	2.672	3.185	4.041	44.5	1.595	2.833	3.377	4.285
46.2	1.524	2.697	3.214	4.077	45.5	1.611	2.855	3.403	4.317
47.4	1.541	2.721	3.243	4.112	46.5	1.627	2.877	3.429	4.349
47.9	1.548	2.731	3.254	4.127	47.5	1.642	2.899	3.454	4.380
48.5	1.557	2.743	3.268	4.145	48.5	1.657	2.920	3.479	4.412
49.1	1.565	2.755	3.282	4.162	49.5	1.672	2.941	3.503	4.442
49.6	1.572	2.765	3.294	4.176	49.6	1.673	2.943	3.506	4.445
50.0	1.578	2.773	3.303	4.188	50.0	1.679	2.952	3.515	4.457

Table 4. Maximum Radius of the Bubble (r_{max}) in μm at Various Retinal Radiant Exposure (H_0) for Rabbit at Two Different q Values Calculated Using Ideal Gas Law and Van Der Waals Equation

r_{max} for $q = 2770$ J g^{-1}					r_{max} for $q = 2297$ J g^{-1}				
H_0 (J cm^{-2})	$\alpha = 120$ cm^{-1}	$\alpha = 526$ cm^{-1}	$\alpha = 821$ cm^{-1}	$\alpha = 1587$ cm^{-1}	H_0 (J cm^{-2})	$\alpha = 120$ cm^{-1}	$\alpha = 526$ cm^{-1}	$\alpha = 821$ cm^{-1}	$\alpha = 1587$ cm^{-1}
0.7				0.000	0.7				0.001
0.8				0.384	0.8				0.502
1.4			0.000	1.012	1.4			0.001	1.078
1.5			0.444	1.064	1.5			0.468	1.131
2.2		0.000	0.858	1.309	2.2		0.000	0.914	1.394
2.5		0.563	0.969	1.404	2.5		0.596	1.030	1.494
3.5		0.891	1.201	1.630	3.5		0.947	1.277	1.735
5.5		1.209	1.500	1.954	5.5		1.286	1.596	2.080
6.5		1.319	1.613	2.082	6.5		1.404	1.716	2.216
8.5		1.497	1.801	2.300	8.5		1.593	1.916	2.448
9.4	0.000	1.565	1.874	2.386	9.4	0.000	1.667	1.997	2.542
9.5	0.223	1.572	1.881	2.394	9.5	0.216	1.673	2.002	2.548
10.5	0.510	1.640	1.956	2.482	10.5	0.539	1.745	2.081	2.642
12.5	0.722	1.762	2.090	2.641	12.5	0.766	1.875	2.224	2.811
14.5	0.852	1.869	2.208	2.783	14.5	0.906	1.989	2.350	2.962
17.5	0.995	2.010	2.365	2.972	17.5	1.058	2.139	2.517	3.163
18.5	1.034	2.052	2.413	3.030	18.5	1.100	2.184	2.568	3.225
20.5	1.105	2.133	2.504	3.140	20.5	1.175	2.270	2.665	3.342
21.5	1.137	2.171	2.547	3.192	21.5	1.210	2.311	2.711	3.397
22.5	1.168	2.208	2.588	3.242	22.5	1.242	2.350	2.755	3.451
23.5	1.197	2.243	2.628	3.291	23.5	1.273	2.388	2.798	3.503
24.5	1.224	2.278	2.667	3.338	24.5	1.303	2.424	2.839	3.553

25.5	1.251	2.311	2.705	3.385	25.5	1.331	2.460	2.880	3.603
26.5	1.276	2.344	2.742	3.430	26.5	1.358	2.495	2.919	3.650
27.5	1.301	2.376	2.778	3.473	27.5	1.384	2.529	2.957	3.697
28.5	1.324	2.407	2.813	3.516	28.5	1.409	2.561	2.994	3.742
29.5	1.347	2.437	2.847	3.558	29.5	1.433	2.593	3.031	3.787
30.5	1.369	2.466	2.881	3.599	30.5	1.457	2.625	3.066	3.830
31.5	1.390	2.495	2.913	3.638	31.5	1.479	2.655	3.101	3.873
32.5	1.411	2.523	2.945	3.677	32.5	1.501	2.685	3.135	3.914
33.5	1.431	2.550	2.977	3.716	33.5	1.523	2.714	3.168	3.955
34.5	1.451	2.577	3.007	3.753	34.5	1.544	2.743	3.201	3.995
35.5	1.470	2.603	3.037	3.790	35.5	1.564	2.771	3.233	4.034
36.5	1.488	2.629	3.067	3.826	36.5	1.584	2.798	3.264	4.072
37.5	1.506	2.654	3.095	3.861	37.5	1.603	2.825	3.295	4.110
38.5	1.524	2.679	3.124	3.896	38.5	1.622	2.851	3.325	4.147
39.5	1.541	2.703	3.152	3.930	39.5	1.640	2.877	3.354	4.183
40.5	1.558	2.727	3.179	3.963	40.5	1.658	2.903	3.384	4.218
41.5	1.575	2.751	3.206	3.996	41.5	1.676	2.928	3.412	4.254
42.5	1.591	2.774	3.232	4.029	42.5	1.693	2.953	3.440	4.288
44.5	1.622	2.819	3.284	4.092	44.5	1.726	3.001	3.495	4.355
46.5	1.652	2.863	3.334	4.153	46.5	1.759	3.047	3.548	4.421
48.5	1.682	2.905	3.382	4.213	48.5	1.790	3.092	3.600	4.484
50.5	1.710	2.946	3.430	4.271	50.5	1.820	3.136	3.650	4.546
53.5	1.750	3.006	3.498	4.355	53.5	1.863	3.200	3.723	4.636
55.0	1.770	3.035	3.531	4.396	55.0	1.884	3.231	3.759	4.679

Table 5. Relative Dimension of Retinal Pigment Epithelial Cells of Monkeys, Rabbits, and Human[35]. Human Cell Dimension is also Provided for Comparison

Species	Average RPE Cell Diameter (μm)	Average RPE Cell Height (μm)	Volume $(\mu m)^3$
Monkey	12	10	1130.97
Rabbit	22	6	2280.80
Human	14	10	1539.38

Table 6. Mean Number of Melanosomes per RPE Cell Profile from Three Retinal Zones Namely Macular, Equator, and Peripheral of 50 Human Eyes Five from each 10 Decades of Life[43]

	Mean Number of Melanosome			
Age (Yrs)	Macula	Equatorial	Peripheral	Total
1–20	17.6	18.4	29.9	65.9
21–60	13.3	12.7	22.2	48.2
61–100	11.1	13.3	15.0	39.4

RPE cell volume. This corresponds to the volume 565.49 μm^3 for monkey and 1140.40 μm^3 for rabbit. The radius of the damaging sphere to cause threshold damage in monkey and rabbit, respectively are calculated to be 1.383 μm and 1.748 μm. In the present work, we report the ED_{50} values calculated for the four laser wavelengths considering the shape of the melanosome as hexagonal and cylindrical. Our calculated ED_{50} values for the laser wavelengths at 0.514 μm, 0.633 μm, 0.694 μm and 1.060 μm are given in Table 7, along with the experimentally observed ED_{50} values (Table 8 and 9) for the laser wavelengths at 0.694 μm and 1.060 μm. It is important to emphasize that our model, which utilizes bubble formation as a damage mechanism, is valid for pulses in the range 10^{-6} to 10^{-9} s. Hence, we compare our calculated ED_{50} values with the experimentally observed ED_{50} for lasers with the pulse duration in the above-mentioned range. Since, Ar^+ laser at 0.514 μm and the He-Ne laser at 0.633 μm operate in continuous wave (CW) mode, pulses in the 10^{-6} to 10^{-9} s range cannot be achievable. However, our calculated ED_{50} values at 0.514 μm can be compared to the experimentally observed ED_{50} at 0.532 μm, which is the closest wavelength available in the desired pulse range.

Let us compare a few experimentally observed ED_{50} retinal exposure that are presented in Tables 8 and 9 with our calculated values (Table 7).

Table 7. Retinal Radiant Exposure Calculated for Two Different Types of RPE Cells at Four Different Absorption Coefficient for Both Monkey and Rabbit at Two q Values

Monkey					Rabbit				
	H_0 (J cm^{-2})					H_0 (J cm^{-2})			
	Hexagonal		Cylindrical			Hexagonal		Cylindrical	
	$r_{max} = 1.298\ \mu m$		$r_{max} = 1.383\ \mu m$			$r_{max} = 1.641\ \mu m$		$r_{max} = 1.746\ \mu m$	
α (cm^{-1})	q = 2770 J g^{-1}	q = 2297 J g^{-1}	q = 2770 J g^{-1}	q = 2297 J g^{-1}	α (cm^{-1})	q = 2770 J g^{-1}	q = 2297 J g^{-1}	q = 2770 J g^{-1}	q = 2297 J g^{-1}
100	32.870	29.215	37.390	32.96	120	45.710	39.530	53.290	45.820
446	7.420	6.593	8.438	7.438	526	10.510	9.087	12.250	10.533
742	4.484	3.985	5.100	4.496	821	6.770	5.854	7.892	6.786
1510	2.235	1.986	2.542	2.241	1587	3.550	3.072	4.142	3.561

Table 8. Comparison of Calculated ED_{50} Values for Monkeys (Macaca Mulatta) at Different Laser Wavelengths with the Values Available in the Literature

Laser Wavelength (μm)	Pulse Duration (ns)	Retinal Image Size (μm)	ED_{50} Values from Literature		Method	H_0 (J cm^{-2}) Calculated
			Energy (μJ)	Radiant Exposure (J cm^{-2})		
0.694	10	20–25	22	7.00–4.48	Opthalmoscopy[53]	8.438^{ω} $7.420^{\perp}$
	20	50	34	1.73	Opthalmoscopy[14]	
	40	30	16	2.26	Opthalmoscopy[49]	
		150	48.3	0.27		
		30	2.9	0.41	Fluorescein[49]	
		150	14.1	0.08		
1.060	100	30	190	26.88	Opthalmoscopy[14]	37.390^{ω} $32.870^{\perp}$
	5			0.00432	Maximum likelihood method[51]	
	15	25	80	16.30	Opthalmoscopy[50]	
		50	68	3.46		
		30	135	19.10	Opthalmoscopy[49]	
			47	6.65	Fluorescein[49]	

		175	1094	4.55	Opthalmoscopy[49]	
			336	1.40	Fluorescein[49]	
	30	90–100	280	4.40–3.57	Opthalmoscopy[53]	
0.532	4	30	1.5	0.21	Opthalmoscopy[55]	$2.542^{\varepsilon\omega}$ $2.235^{\varepsilon\perp}$
	40	250	30.5	0.06	Fluorescein angiography[54]	
			50.0	0.10	visual[54]	

[ε]Value at $8 = 0.514\,\mu m$.
[ω]Cylindrical shape.
[⊥]Hexagonal shape.

Table 9. Comparison of Calculated ED_{50} Values for Rabbits (Chinchilla Grey) at Different Laser Wavelengths with the Values Available in the Literature

Laser Wavelength (μm)	Pulse duration (ns)	Retinal Image Size (μm)	ED_{50} Values from Literature		Method	Calculated Retinal Radiant Exposure (J cm^{-2})
			Energy (μJ)	Radiant Exposure (J cm^{-2})		
0.694	20	33	7.8	0.91	Opthalmoscopy[14]	12.250^{ω} $10.510^{\perp}$
	30	800		0.07	Opthalmoscopy[47]	
	80	250		0.0045	Opthalmoscopy[48]	
1.060	100	20	36	11.46	Opthalmoscopy[14]	53.290^{ω} $45.710^{\perp}$
	5			0.0012	Maximum likelihood method[51]	
0.532	4	30	5	0.71	Opthalmoscopy[52]	$4.142^{\varepsilon\omega}$ $3.550^{\varepsilon\perp}$
	40	200	7.8	0.02	Fluorescein angiography[54]	

[ε]Value at $8 = 0.514\,\mu m$.
[ω]Cylindrical shape.
[⊥]Hexagonal shape.

The calculated ED_{50} values for both monkey and rabbit at a wavelength of 0.694 μm are 8.438 and 12.250 J cm^{-2}, considering the shape of the melanosome to be cylindrical and 7.420 and 10.510 J cm^{-2} for hexagonal shape. Birnguber *et al.*[14] has obtained experimentally ED_{50} value to be 1.73 J cm^{-2} for macaca mulatta monkey using a ruby laser at wavelength 0.694 μm with 20 μs pulse. It should also be noted that the ED_{50} threshold energy was 34 ± 4 μJ and beam spot size of 50 μm. The same authors observed ED_{50} value for chinchilla grey rabbit to be 0.91 J cm^{-2}. In this case the retinal injury threshold was 7.8 ± 1.5 μJ for a laser spot size of 33 μm. From Table 8, it is evident that our calculated values for retinal radiant exposure are 4.9 (cylindrical shape) and 4.3 (hexagonal shape) times greater for monkey and 13.5 (cylindrical shape) and 11.5 (hexagonal shape) times greater for rabbit than the observed values when the ideal gas law is used to calculate q. This increase narrows to 4.3 (cylindrical shape) and 3.8 times (hexagonal shape) for monkey and 11.6 (cylindrical shape) and 10.0 time (hexagonal shape) when van der Waals equation of state is used. It is important to note that our model does not address the retinal image dependent damage threshold. It has been observed that there exists an inverse relationship between damage threshold and retinal image size over a wide range of laser pulse durations[46]. However this inverse relationship between the damage threshold and retinal image size is not well established as seen in Table 8 and Table 9 for monkeys and rabbits, respectively. In general, the value of the threshold retinal exposure to produce a fluorescein positive lesion is less than the value to produce opthalmoscopically visible lesion.

The threshold retinal radiant exposure value is the highest at Nd:YAG laser wavelength (1.060 μm) for monkey and rabbit compared to that at all other wavelengths used in this investigation due to its lowest absorption coefficient (120 for monkey and 100 cm^{-1} for rabbit). Our calculated ED_{50} values are 37.390 J cm^{-2} and 53.290 J cm^{-2} considering the shape of the melanosome to be cylindrical for monkey and rabbit, respectively as given in Table 7. When calculated for the hexagonal shape the ED_{50} values are 32.870 J cm^2 and 45.710 J cm^2 for monkey and rabbit respectively. Considering the shape of the RPE cells as cylindrical our calculated ED_{50} values are 29.8% and 78% higher than those experimentally observed values of Birngruber *et al.*[14] using 1.060 μm laser of 100 ns pulse with retinal spot size of 30 μm. When q is calculated using van der Waals equation of state this increase narrows to 18.4% for monkeys and 75.0% for rabbit. Ham *et al.*[50] reported lower ED_{50} values for shorter pulses of duration 15 ns in doing experiments on rhesus monkey. Their value was 3.46 ± 0.61 J cm^{-2} for the retinal image size of 25 μm. It is worth mentioning that their standard deviation in the ED_{50} value was

18% and the threshold lesion usually appeared 24 hrs. after laser exposure and the estimated retinal image size varied in the range 25—50 μm. Jiemin *et al.*[51] reported ED_{50} values for both monkey and rabbit as 4.32 and 1.21 mJ cm^{-2} using a Nd:YAG having a 5 ns laser pulse. The authors did not report the retinal image size. Their values are more than two orders of magnitude smaller than that of Birngruber *et al*[14]. The ratio of the value of the retinal damage ED_{50}, for rabbit to monkey at 1.060 μm is 1:3.6. The ratio obtained in the present work is 1:0.70, whereas Birngruber *et al.*[14] reported it as 1:2.3. It is extremely difficult to pulse Ar^{+} laser and He-Ne laser into micro-second or nano-second range and hence at these laser wavelengths no ED_{50} values are available in the pulse range at which our model is valid. However, if one compares the ED_{50} values of 0.71 J cm^{-2} reported by Toth *et al.*[52] for 0.532 μm laser with 4 ns pulse and 30 μm retinal spot size, the ED_{50} values reported in the present work at 0.514 μm is 5.8 times higher.

CONCLUSION

In the present work, we have used an adiabatic model for laser induced bubble formation as a damage mechanism in the retinas of monkeys and rabbits. The growth of the bubble was calculated using the ideal gas law. Our ED_{50} values are compared with the experimental values available in the literature for pulse duration in the sub-micro-second to nano-second time scales which are relevant to this model. Our calculated ED_{50} values are in reasonable agreement with Birngruber *et al.*[14] for the lasers at 0.694 μm and 1.060 μm with pulse durations in the time scale for which the model is valid. When q was calculated using van der Waals equation of state to derive ED_{50} values, the deviation observed between our calculated and experimentally observed ED_{50} values was found to be narrowed. Our ED_{50} values at 0.514 μm and 0.633 μm are not compared due to unavailable data in the pulse duration of 10^{-6} to 10^{-9} s. The large deviation of our ED_{50} values from other investigations may be attributed to the wide variation in their measurements on retinal image size. In addition, our estimation of retinal radiant exposure from the threshold energy and retinal image size is based on the assumption that their beam profile is gaussian (TEM_{00}). Our results suggest that the thermodynamic model using the van der Waals equation of state may predict more accurately the laser induced retinal damage due to bubble formation than the model using the ideal gas equation.

APPENDIX

The energy required to raise 1 gm of H_2O from 37 °C @ 1 atm. to critical temperature (374 °C) @ 218 atm. can be calculated using the thermodynamic relation:

$$\Delta U = \Delta H - \Delta(PV).$$

At 1 atm. the vapor can be treated as an ideal gas.
ΔH @ 1 atm. (constant): $T_1 = 37\,^\circ C \rightarrow T_2 = 374\,^\circ C$

$$\Delta H = 3066\,J\,g^{-1}$$

ΔH @ T (constant) = 647 °C; $P_1 = 1$ atm. $\rightarrow P_2 = 218$ atm.

$$\Delta H_{ideal} = \Delta U_{ideal} + \Delta(PV)_{ideal}$$
$$= -230\,J\,g^{-1} \text{ (where } \Delta U_{ideal} = 0)$$

$(\Delta P)_{overall} = 70\,J\,g^{-1}$ (ideal gas law can still be valid).
Using van der Waals equation, ΔH @ T (constant) = 647 °C; $P_1 = 1$ atm. $\rightarrow$ $P_2 = 218$ atm.

$$\Delta H_{van\ der\ Waals} = \Delta U_{van\ der\ Waals} + \Delta(PV)_{van\ der\ Waals}$$

$$\Delta U_{van\ der\ Waals} = an^2\left(\frac{1}{v_1} - \frac{1}{v_2}\right) = -409.88\,J\,g^{-1}$$

$$\Delta(PV)_{van\ der\ Waals} = n^2bRT\left(\frac{1}{v_2 - nb} - \frac{1}{v_1 - nb}\right) + n^2a\left(\frac{1}{v_1 - v_2}\right)$$

$$\Delta H_{van\ der\ Waals} = 2\,U + n^2bRT\left(\frac{1}{v_2 - nb} - \frac{1}{v_1 - nb}\right) = -699\,J\,g^{-1}$$

$$q_{van\ der\ Waals} = 2297\,J\,g^{-1}$$

$$q_{ideal} = 2770\,J\,g^{-1} \text{ (calculated in ref. 33)}$$

ACKNOWLEDGMENT

We gratefully acknowledge the financial support of ONR Grant No. 0014-1-0523.

REFERENCES

1. Moseley, H.; Allan, D. Phys. Med. Biol. **1987**, *32*, 1159.
2. March, W.F.; Gherezghiher, T.; Shaver, R.P.; Kauss, M.C.; Norquist, R.E. Lasers Surg Med. **1987**, *6*, 584.

3. Frankhauser, F.; Roussel, P.; Stebban, J.; Van der Zypen, E. Int. Opthal. **1981**, *3*, 129.
4. Sartori, S.; Henry, P.D.; Sauerbreg, R.; Tittel, F.K. Lasers Surg Med. **1987**, *7*, 300.
5. Grundfest, W.S.; Litvack, F.; Hickey, A. J. Vasc. Surg. **1988**, *5*, 667.
6. Inser, J.M.; Steg, P.G.; Clarke, R.H. IEEE J. Quantum Electron. **1987**, *23*, 1756.
7. Lee, G.; Ikeda, R.M.; Theis, J.H.; Chan, M.C.; Stubble, D.; Ogata, D.; Kugagai, A.; Mason, D.A. Am. J. Cardiol. **1984**, *53*, 290.
8. Walsh, J.T.; Flute, T.J.; Deutsch, T.F. Lasers Surg Med. **1989**, *9*, 314.
9. Vogel, A.; Busch, S.; Jungnickel, K.; Birngruber, R. Lasers Surg Med. **1994**, *15*, 32.
10. Lin, C.P.; Weaven, Y.K.; Birngruber, R.; Fujimoto, J.G.; Puliafito, C.A. Lasers Surg Med. **1994**, *15*, 44.
11. Rink, K.; Delacretaz, G.; Salase, R. Lasers Surg Med. **1995**, *16*, 134.
12. Sentrayan, K.; Thorpe, Jr., A.; Michael, A.; Trouth, C.O. Spect. Lett. **1998**, *31*, 559.
13. Joly, M. *A Physio-Chemical Approach to the Denaturation of Proteins*; Academic Press: New York, 1965.
14. Birngruber, R.; Hillenkamp, F.; Gabel, V.P. Health Phys. **1985**, *48*, 781.
15. Zysset, B.; Fujimoto, J.G.; Deutsch, T.F. Appl. Phys. **1989**, *B 48*, 139.
16. Fujimoto, J.G.; Lin, W.Z.; Ippen, E.P.; Puliafito, C.A.; Steinert, R.F. Invest. Optical. Vis. Sci. **1985**, *26*, 1771.
17. Doukas, A.G.; Zweig, A.G.; Frisoli, J.K.; Birngruber, R.; Deutsch, T.F. Appl. Phys. **1989**, *B 53*, 237.
18. Vogel, A.; Busch, S.; Jungnickel, K.; Birngruber, R. Lasers Surg Med. **1994**, *15*, 43.
19. Doukas, A.G.; McAuliffe, D.J.; Flotte, T.J. Ultrasound Med. Biol. **1993**, *19*, 137.
20. Wantanabe, S.; Flotte, T.J.; McAuliffe, D.J.; Jacques, S.L. Invest. Dermatol. **1993**, *90*, 761.
21. Zweig, A.D.; Venugopalan, V.; Deutsch, T.F. Appl. Phys. **1993**, *74*, 1481.
22. Kaver, I.; Koontz, Jr. W.W.; Wilson, J.D.; Guice, J.M.; Smith, J.M. J. Urol **1992**, *147*, 219.
23. Smith, F.L.; Carper, S.W.; Halls, J.S.; Gilligan, B.J.; Madsen, E.L.; Storm, F.K.J. Urol **1992**, *147*, 486.
24. Yashima, Y.; McAuliffe, D.J.; Jacques, S.L.; Flotte, T.J. Lasers Surg Med. **1991**, *11*, 62.
25. Niemz, M.H.; Hoppeler, T.; Juhasz, T.; Bille, J.F. Light Opthal. **1993**, *5*, 145.

26. Stern, D.; Schoenlein, R.W.; Puliafito, C.A.; Dobi, E.T.; Birngruber, R.; Fujimoto, J.G. Arch. Opthal. **1989**, *107*, 587.
27. Flotte, T.J.; Frisoli, J.K.; Goetschkes, M.; Doukas, A.G. Laser Induced Shockwave Effect on Red Blood Cells. In *Laser-Tissue Interaction II*; SPIE, 1991; 1427–1436.
28. Hansen, W.P.; Fine, S. Appl. Opt. **1968**, *7*, 155.
29. van Leeuwen, T.G.; vand der Veen, M.J.; Verdaasdonk, R.M.; Borst, C. Lasers Surg Med. **1991**, *11*, 26.
30. Asshauser, T.; Rink, K.; Kelacretaz, G. J. Appl. Phys. **1994**, *76*, 5007.
31. Frenz, M.; Pratiso, H.; Ith, M.; Asshauser, T.; Rink, K.; Delacreatz, G.; Romano, V.; Salathe, R.P.; Weber, H.P. In *Laser Tissue Interaction III*; Jacques, S.L., Katzin, A. Eds.; Bellingham, WA, SPIE, 1994; 402.
32. Rodes, J.W. Laser Induced Hemorrhagic Lesions: A Reviews of Accidental Injuries and Related Experimental Findings in Animals. **1993**, *5*, 211.
33. Gerstman, B.S.; Thompson, C.R.; Jacques, S.L.; Rogers, M.K. Lasers Surg. Med. **1996**, *18*, 10.
34. Cleary, S.F. Laser Pulse and the Generation of Acoustic Transients in Biological Materials. In *Laser Applications in Medical Biology*; Wolbarsht, M.L. Ed.; Plenum Press: New York, 1977; 3, 175.
35. Ts'o, M.O.M.; Friedman, E. Arch. Opthal. **1967**, *78*, 641.
36. Docchio, F. Lasers Surg Med. **1989**, *9*, 515.
37. Feeney, L. Invest. Opthalmol. Vis. Sci. **1978**, *216*, 563.
38. Eldred, G.E.; Katz, M.L. Exp. Eye Res. **1988**, *47*, 71.
39. Cubeddu, R.; Docchio, F.; Ramponi, R.; Boulton, M. IEEE J. Quant. Elect. **1990**, *26*, 2218.
40. Feeney, L.; Grieshaber, J.H.; Hogen, M.J. Studies on Human Ocular Pigment. In *Structure of Eye*; Rohen J.W. Ed.; Schattuer-Verlag: Stuttgart, 1965.
41. Mellerio, J. Exp. Eye Res. **1966**, *242*, 242.
42. Welch, A.J. IEEE Trans. Bio. Med. Engg. **1984**, *36*, 633.
43. Burns, L.F.; Hilderbrand, E.S.; Eldridge, S. Invest. Opthal. Vis. Sci. **1984**, *25*, 195.
44. Gabel, V.P.; Birngruber, R.; Hillenkamp, F. Gesellschaft fúr strahlen – und Umwelt-forschung mbh, 1976.
45. Birngruber, R.; Puliafito, C.A.; Gawande, A.; Lin, W.Z.; Schoelein, R.W.; Fujimoto, J.G. IEEE J. Quantum Electron. **1987**, *QE- 23*, 1836.
46. Sliney, D.H.; Wolbarsht, M.L. *Safety with Lasers and Other Optical Sources*; Plenum: New York, 1980; 130.
47. Ham, Jr. W.T. Occular Effects of Laser Radiation Part I. DASA Rept. **1964**, 1574.

48. Kohtiao, A.; Resnick, I.; Newton, J.; Schwell, H. Am. J. Opthalmol. **1966**, *62*, 644.
49. Borland, R.G.; Brennan, D.H.; Marshall, J.; Viveash, J.P. Expt. Eye Res. **1978**, *27*, 471.
50. Ham, Jr. W.T.; Mueller, H.A.; Goldman, A.I.; Newman, B.E.; Holland, L.M. Kuwabara, T. Science. **1974**, *185*, 362.
51. Jiemin, X.; Guidao, X.; Zhongli, C.; Liangshun, S.; Fugen, H.; Shuying, Z.; Huanwen, Q.; Guisu, Z.; Denglong, W.; Haifeng, L.; Guanghuang, G.; Dechang, W. Health Phys. **1989**, *56*, 647.
52. Toth, C.A.; Cain, C.P.; Stein, C.D.; Noojin, G.D.; Stolarski, D.J.; Zuclich, J.A.; Roach, P. Invest. Opthalmol. Vis. Sci. **1995**, *36*, 1910.
53. Vassiliadis, A.; Zweng, H.C.; Peppers, N.A.; Peabody, R.P. Arch. Envirn. Health **1970**, *20*, 161.
54. Courant, D.; Court, L.; Abadie, B.; Brouillet, B. Health Phys. **1989**, *56*, 637.
55. Cain, C.P.; Toth, C.A.; DiCarlo, C.D.; Stein, C.D.; Noojin, G.D.; Stolarski, D.J.; Roach, W.P. Invest. Opthalmol. Vis. Sci. **1995**, *36*, 879.

Received November 5, 2000
Accepted February 15, 2001